ISSN 1063-7710, Acoustical Physics, 2021, Vol. 67, No. 1, pp. 26–37. © Pleiades Publishing, Ltd., 2021.
Russian Text © The Author(s), 2021, published in Akusticheskii Zhurnal, 2021, Vol. 67, No. 1, pp. 31–44.

NONLINEAR ACOUSTICS

Numerical Simulation of a Nonlinear Parabolic Equation for Analyzing The Perceived Loudness Statistics of Sonic Boom Wave after Propagation Through Atmospheric Turbulent Layer

P. V. Yuldashev[a], *, M. M. Karzova[a], **, V. A. Khokhlova[a], *, and Ph. Blanc-Benon[b], ******

[a] *Physics Faculty, Moscow State University, Moscow, 119991 Russia*

[b] *LMFA, UMR 5509, Ecole Centrale de Lyon, CNRS, Université de Lyon, 36 Avenue Guy de Collongue, 69134, Ecully, Cedex, France*

**e-mail: petr@acs366.phys.msu.ru*

***e-mail: masha@acs366.phys.msu.ru*

****e-mail: vera@acs366.phys.msu.ru*

*****e-mail: philippe.blanc-benon@ec-lyon.fr*

Received April 21, 2020; revised August 31, 2020; accepted September 8, 2020

Abstract—Sonic boom propagation in the atmospheric turbulent layer, represented by a model of homogeneous isotropic turbulence, is investigated numerically in two-dimensional geometry using a KZK-type nonlinear parabolic equation for an inhomogeneous moving medium with relaxation. The mean value, standard deviation, and cumulative probabilities of the sonic boom amplitude, shock front steepness, and the Perceived Loudness Mark VII metric of subjective loudness of an impulse noise are analyzed at different propagation distances traveled by the sonic boom wave in the turbulent layer and for different initial amplitudes of the wave.

Keywords: sonic boom, KZK equation, turbulence, impulse noise loudness

DOI: 10.1134/S1063771021010061

1. INTRODUCTION

Research on the sonic boom problem dates back to more than 60 years ago [1]. Sonic boom is a pulsed acoustic perturbation with a shock front generated by supersonic aircraft that propagates as a Mach cone to the Earth's surface [2]. The classic waveform of the sonic boom wave resembles the letter *N* and is conventionally called an *N*-wave [3]. Such a shock wave is perceived by people as an extremely sharp and annoying impulse noise [4]. This is the main reason why supersonic flights of civil aircrafts are prohibited over populated areas [5]. In the last decade, sonic boom research activity has been associated with plans to create supersonic business-class passenger aircrafts, that are approximately two times smaller in size than the Concorde [5–7]. Currently, the main efforts are aimed at optimizing fuselage shape to modify the resulting waveform and minimize the impact of its generated impulse noise [8–10]. Although there have been efforts to minimize the impact of sonic boom since the earliest development of supersonic flights [1, 5], significant progress in this area is related to the evolution of computational aerodynamics methods and increase in computer processing power [11].

The resulting pressure wave signature of the sonic boom at the Earth's surface is governed not only by the aerodynamic processes by which an aircraft generates a shock wave. In the final segment of the propagation trajectory from the aircraft's altitude to the ground, a sonic boom wave passes through the surface turbulent layer of the thickness that can reach 1–2 km [12]. Due to the oblique incidence of the wave in the form of a Mach cone on the ground and due to refraction in a stratified atmosphere, the path traversed by the shock wave in the surface turbulent layer can be several times longer than its thickness [13]. Acoustic inhomogeneities caused by random fluctuations in wind speed and temperature in an unstable atmosphere lead to random focusing and defocusing of the acoustic field [14, 15]. As a result, the acoustic field acquires a complex random spatiotemporal structure. The effects related to propagation through a turbulent layer have been observed many times under natural conditions [13, 16, 17] and have also been widely studied in model experiments under laboratory conditions [18–20]. It has been shown that with an increase in the thickness of the turbulent layer and an increase in fluctuations in the sound speed, the standard deviation of the shock wave amplitude increases up to a certain limit. In this

case, the rise time of the shock front also increases on average in comparison with the values obtained in a homogeneous medium.

For a finer analysis of the processes occurring during propagation of a shock wave through a turbulent layer, numerical experiments were carried out with various theoretical models [10, 21–32]. Previously, methods involving the geometric acoustics of inhomogeneous media were widely used [10, 21–25]. To account for diffraction effects, various one-way wave equations have been applied. Among these equations, a nonlinear parabolic KZK (Khokhlov–Zabolotskaya–Kuznetsov) type equation that takes into account the vector and scalar inhomogeneities of the propagation medium and the relaxation mechanism of absorption, has been broadly used [26–30]. More complex wide-angle parabolic models have also been developed [31, 32] but remain unpopularized. The theoretical studies covered the statistics of the wave amplitude, the rise time of the shock front, as well as its steepness, as a function of the initial sonic boom parameters and the distance traveled in the turbulent layer. It has been shown that the wave amplitude can, with a probability of several percent, increase by a factor of two or more with respect to the nominal level [27–30]. Scattering by turbulent inhomogeneities mainly leads to blurring of the shock front, which can be partially compensated by nonlinear effects [30].

For noise level standards, it is not the physical characteristics of the shock pulse on the Earth's surface that are of importance, but its subjective perception [17, 33]. From psychoacoustic studies, it is known that the amplitude and rise time of the shock front of a sonic boom wave are primarily responsible for the perceived noise level [34]. To estimate this level, various metrics can be used, most of which are calculated from the spectral power of the waveform [35]. One of the commonly used metrics of the perceived noise level of sonic boom is the Perceived Loudness Mark VII (abbreviated PL) [36–38], which correlates well with the subjective loudness rating level [35] and has become the de facto standard in this research [38].

There have been relatively few studies evaluating the effect of turbulence on the perceived noise level of sonic boom [29, 39], and much remains uncertain in this field. On the other hand, it is extremely important for regulators to estimate the noise level spread [4]. Therefore, the aim of this work was a theoretical study of the PL statistics of an *N*-wave after propagation through a turbulent layer and its comparison with statistics of the wave amplitude and shock front steepness that have been studied in more details. For this purpose, a theoretical model based on a nonlinear parabolic equation for an inhomogeneous moving medium was used [26–30]. As a result of solving this equation using numerical modeling methods, the *N*-wave waveforms randomly distorted due to refraction by wind speed inhomogeneities in homogeneous isotropic turbulence, were obtained. The PL, amplitude, and shock front steepness values calculated for each waveform were analyzed statistically for *N*-waves of different amplitudes and at different propagation distances in depth of the turbulent layer.

2. THEORETICAL METHOD

2.1. Nonlinear Parabolic Equation in an Inhomogeneous Moving Medium

To calculate the sound field as an *N*-wave propagates through the turbulent layer, a nonlinear parabolic KZK-type equation for an inhomogeneous moving medium was used in a two-dimensional geometry [26]:

$$\frac{\partial p}{\partial z} = \frac{c_0}{2}\int_{-\infty}^{\tau}\frac{\partial^2 p}{\partial x^2}d\tau' - \frac{n^2-1}{2c_0}\frac{\partial p}{\partial \tau} + \frac{u_{0z}}{c_0^2}\frac{\partial p}{\partial \tau} + \frac{u_{0x}}{c_0}\frac{\partial p}{\partial x} + \frac{\varepsilon}{\rho_0 c_0^3}p\frac{\partial p}{\partial \tau} + \frac{\delta}{2c_0^3}\frac{\partial^2 p}{\partial \tau^2} + L_{\text{relax}}(p). \quad (1)$$

Here p is the acoustic pressure, z is the longitudinal coordinate along the main direction of wave propagation, x is the transverse coordinate, t is time, c_0 and ρ_0 are the ambient sound speed and air density, $\tau = z - t/c_0$ is the time in the retarded time coordinate system, τ' is an auxiliary integration variable, u_{0z} and u_{0x} are the longitudinal and transverse components of the wind speed vector $\mathbf{u}$, δ and ε are the coefficients of thermoviscous absorption and nonlinearity in air, respectively, and $n = c_0/c$ is the refractive index for scalar inhomogeneities.

The terms on the right-hand side of the equation (1) sequentially describe the physical effects related to diffraction, scalar inhomogeneities, wave convection along the longitudinal and transverse directions, acoustic nonlinearity, and thermoviscous absorption. The last term in the equation, which is the integro-differential operator

$$L_{\text{relax}}(p) = \sum_j^J d_j \frac{\partial}{\partial \tau}\int_{-\infty}^{\tau}\exp\left(-\frac{\tau-\tau'}{\tau_j}\right)\frac{\partial p}{\partial \tau'}d\tau', \quad (2)$$

takes into account absorption and dispersion caused by relaxation processes due to excitation of the vibrational degrees of freedom of nitrogen and oxygen molecules ($J = 2$) [40]. The relaxation process with the subscript j is characterized by the difference between the sound speed in nonequilibrium and equilibrium states $\Delta c_j = d_j c_0^2$ and the relaxation time τ_j. To simplify the equation, the terms related to inhomogeneities of the density of the medium are omitted, since they have a weak effect on the acoustic field against the refractive effects of an inhomogeneous medium. The equation is obtained with first-order accuracy in the Mach number for wind speed $M = |\mathbf{u}|/c_0$, which is about 10^{-2} for the planetary turbulent layer. The acoustic Mach

number is also assumed to be small and for sonic boom waves is usually less than 10^{-3}. The equation is valid when the diffraction angles are small with respect to the initial direction of wave propagation (usually no more than 15°) and when fluctuations in the parameters of inhomogeneities are smooth and small.

2.2. Parameters of the Medium and Homogeneous Isotropic Turbulence Model

The acoustic parameters of air were calculated for a temperature of 20°C, a relative humidity of 25%, and a pressure of 10^5 Pa and yielded $c_0 = 343.8$ m/s, $\rho_0 = 1.18$ kg/m^3, $\varepsilon = 1.2$, $\delta = 3.85 \times 10^{-5}$ m^2/s. The parameters of relaxation processes for nitrogen and oxygen molecules were $\Delta c_1 = 0.1204$ m/s, $\tau_1 = 9.6$ μs (oxygen), $\Delta c_2 = 0.0219$ m/s, $\tau_2 = 753.7$ μs (nitrogen) [40].

Inhomogeneities of the atmospheric boundary layer were created using a model of two-dimensional homogeneous isotropic kinematic turbulence with a von Karman-type energy spectrum [41]:

$$E(K) = \frac{5}{3}\frac{11}{6}\frac{\left\langle u_{0z}^2 \right\rangle}{c_0^2}\frac{K^3}{L_0^{5/3}}\frac{\exp\left(-K^2/K_m^2\right)}{\left(K^2 + K_0^2\right)^{17/6}}. \qquad (3)$$

Here, $K = \sqrt{K_x^2 + K_z^2}$ is the modulus of the spatial wavenumber, K_x and K_z are the transverse and longitudinal spatial wavenumbers, respectively; $L_0 = 100$ m is the outer turbulence scale, corresponding to the largest-scale turbulence fluctuations, $K_0 = 1/L_0$; $l_0 = 0.01$ m is the inner scale; and K_m is the Kolmogorov scale related to the inner scale l_0 ($K_m = 5.92/l_0$), $\sqrt{\left\langle u_{0z}^2 \right\rangle}$ is the RMS velocity of turbulent pulsations of the longitudinal wind component. The $\sqrt{\left\langle u_{0z}^2 \right\rangle}$ value was chosen equal to 1.7 m/s, which corresponds to the conditions of strong turbulence characteristic to hot deserts in the warm season [29]. In this case the RMS value of fluctuations of effective refractive index $\sqrt{\left\langle u_{0z}^2 \right\rangle}/c_0$ is 0.5%. Near the boundaries of the computational domain, the field of inhomogeneities was gradually zeroed in 200-m-long segments on each side to avoid scattering of the field towards the boundaries and subsequent reflections. The turbulence field changes much more slowly than the characteristic wave travel time; therefore, the wind fluctuation field is considered "frozen," i.e., invariable over time.

Random realizations of the longitudinal and transverse wind speed components u_z and u_x were generated by the method of random Fourier modes [27]. The number of modes was chosen equal to 10000, and their spatial wavenumbers were distributed in the range from 0.314×10^{-4} up to 94.2 m^{-1} in accordance with a logarithmic law [30].

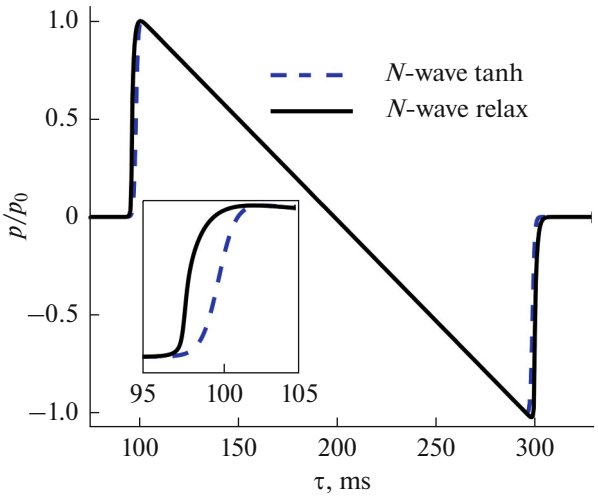

Fig. 1. Initial waveform of symmetrical *N*-wave with shock front structure characteristic to a medium with thermoviscous absorption (dashed curve), and the waveform after its propagation over distance of 6 km in homogeneous atmosphere with account of relaxation and nonlinear effects (solid curve). Pressure waveforms are normalized to initial amplitude $p_0 = 20$ Pa. Inset: differences in structure of shock fronts between the two waveforms.

Scalar inhomogeneities related to temperature fluctuations were not taken into account, and in Eq. (1), the refractive index n was assumed to be equal to 1.

2.3. Initial Wave Field

As the initial acoustic field at the entrance to the turbulent layer, a plane wave with a classical waveform of a symmetric *N*-wave was chosen (Fig. 1). The duration of the wave from the leading to the trailing shock front was $2T_0 = 200$ ms. To study the influence of nonlinear effects, three wave amplitude levels p_0 were considered: 10, 20, and 40 Pa. The first level corresponds to a small business-class aircraft [5], the last is closer to the sonic boom level from full-size Concorde and Tu-144 aircrafts [42]. In this paper, the acoustic pressure is given neglecting reflection from the Earth's surface, which usually doubles the amplitude.

The initial rise time of the shock front τ_{sh}, which is usually defined as a time needed to rise the pressure at the shock front from 10 to 90% of the peak pressure [17, 18, 34], has a large influence on the change in the quantitative parameters of the shock wave as it propagates in a turbulent medium. More specifically, for linear wave focusing, its amplitude in caustics is proportional to the time derivative of the incident waveform. Therefore, the smaller the rise time of the shock front is, the larger the derivative and the greater the increase in the wave amplitude at the focus are [15, 27].

Usually, the waveform of a symmetrical *N*-wave is defined by introducing a function:

$$p(\tau) = p_0 \frac{\tau}{2T_0}\left[-\text{th}\left(\frac{\tau + T_0}{0.455\tau_{sh0}}\right) + \text{th}\left(\frac{\tau - T_0}{0.455\tau_{sh0}}\right)\right], \quad (4)$$

in which a hyperbolic tangent is used to yield a specified rise time τ_{sh0} of the shock front [28]. In this case, positive and negative peak pressures of an *N*-wave are the same, and the leading and trailing shock fronts also have the same structure, which is characteristic for media with a thermoviscous absorption mechanism (Fig. 1, dashed line). In a medium with relaxation, the shock front has a more complex structure [43]; therefore, the following procedure was used to provide a realistic initial waveform. First, for the given parameters of the medium, the propagation of a single shock front of a plane wave was modeled in the form of a pressure step with a given amplitude p_0, to obtain the steady-state value of the rise time of the shock front [44]. For this, a one-dimensional model employing the generalized Burgers equation with relaxation was applied. Such model has been previously used when considering shock pulses from a spark source [45]. Then, the obtained rise time values of the steady shock front were used to determine the waveform of the *N*-wave by the equation (4).

At the final stage, the waveform of the *N*-wave was simulated at a distance of 6 km using the same one-dimensional model, so that the initial structure of the front, a hyperbolic tangent, was transformed to a more realistic form determined by the relaxation effects (Fig. 1, solid line). In this case, the amplitude and the duration of the *N*-wave were selected by an iterative procedure, so that the final initial waveform, which then propagated in the turbulent layer, had the given values of p_0 and T_0. Note that the changes in amplitude and duration of the wave, mainly due to absorption, were less than 3%, and two iterations were sufficient to obtain the final initial values.

The inset to Fig. 1 shows the difference in the structure of the shock front between the waveform determined according to the equation (4) and the waveform obtained in the medium with relaxation for the initial *N*-wave amplitude of $p_0 = 20$ Pa. The above procedure yielded the following rise time values of the shock front: $\tau_{sh} = 3.80$ ms for $p_0 = 10$ Pa, $\tau_{sh} = 1.89$ ms for $p_0 = 20$ Pa, and $\tau_{sh} = 0.92$ ms for $p_0 = 40$ Pa. The average steepness of the front, calculated between the points from which its rise time was computed, for the indicated three cases were 2.1 Pa/ms for $p_0 = 10$ Pa, 8.5 Pa/ms for $p_0 = 20$ Pa, and 35 Pa/ms for $p_0 = 40$ Pa. It is seen, that in the chosen pressure range p_0, the rise time of the shock front is nearly inversely proportional to the amplitude and its steepness is proportional to the amplitude squared [30], although in the general case, when considering a wide range of amplitudes up to several hundred Pa, this is not always the case [44].

2.4. Numerical Algorithm

Equation (1) was solved by the splitting method based on physical factors according to which at each step along the z coordinate, simplified equations are successively solved, on the right-hand sides of which one or more operators of the original equation are taken into account. In this study, the operators were identified as follows:

$$\frac{\partial p}{\partial z} = \frac{c_0}{2}\int_{-\infty}^{\tau}\frac{\partial^2 p}{\partial x^2}d\tau', \quad (5)$$

$$\frac{\partial p}{\partial z} = \frac{u_{0z}}{c_0^2}\frac{\partial p}{\partial \tau}, \quad (6)$$

$$\frac{\partial p}{\partial z} = \frac{u_{0x}}{c_0}\frac{\partial p}{\partial x}, \quad (7)$$

$$\frac{\partial p}{\partial z} = \frac{\varepsilon}{\rho_0 c_0^3} p\frac{\partial p}{\partial \tau}, \quad (8)$$

$$\frac{\partial p}{\partial z} = \frac{\delta}{2c_0^3}\frac{\partial^2 p}{\partial \tau^2} + L_{\text{relax}}(p). \quad (9)$$

Diffraction in the parabolic approximation (5) was calculated in the time domain using the Crank–Nicholson scheme [28–30]. At the boundaries of the numerical domain, boundary conditions in the form of a rigid wall were applied. The convection of the acoustic field in the longitudinal direction (6) was calculated in the frequency domain using the exact analytical solution for each of the temporal harmonics of the waveform. The transverse convection of the acoustic field (7) was calculated using the Lax–Wendroff scheme [26]. Nonlinear effects (8) were calculated using a Godunov-type scheme in the time domain [28]. Thermoviscous absorption and relaxation effects (9) were calculated using the exact analytical solution in the frequency domain. Transition between the temporal and spectral representations of the pressure field was performed using fast discrete Fourier transform (FFT) implemented in the FFTW library.

The steps of the numerical grid along the longitudinal and transverse directions were $\Delta z = 1$ m and $\Delta x = 0.2$ m, respectively. Since the splitting method by physical factors of the second-order of accuracy was used [46], the actual step of the diffraction, convection, and absorption operators was $\Delta z/2 = 0.5$ m. The chosen time grid step $\Delta\tau = 0.016$ ms made it possible to have more than 60 points per shock front for an initial wave with the maximum amplitude considered in the paper. Such a margin in the signal sampling frequency was necessary because of the possible twofold increase in the wave amplitude in the caustics with a corresponding decrease in the rise time of the shock front. The length of the time window was 800 ms, which is equal to four durations of the initial waveform of the *N*-wave. A transverse size of the spatial region of 12800 m was chosen to provide sufficiently long reali-

zations of the acoustic field parameters suitable for statistical analysis. Along the longitudinal coordinate z, calculation was carried out up to a distance of $z_{max} = 2000$ m, which corresponds to the length of the vertical trajectory from the aircraft to the Earth's surface with the largest possible width of the surface turbulent layer.

2.5. Calculation of PL Mark VII and the Steepness of the Shock Front

PL of the sonic boom wave noise level was calculated by the simplified algorithm presented in [37, 38]. The initial data for the algorithm is the signal spectral power in 42 standard one-third octave bands from 1 to 12600 Hz. To obtain the spectral power, a signal with a duration of 800 ms obtained in the calculations was padded with zeros up to the duration of 1625 ms, which made it possible to increase the spectral resolution to 0.8602 Hz. Then, within the boundaries of each one-third octave band, the spectral power was integrated by the trapezoidal method. If the boundaries of one-third octave bands did not coincide with the discrete FFT frequencies, then the spectral power values at these points were obtained by linear interpolation. Then, over the corresponding 42 spectral powers E_f in one-third octave bands, the sound pressure levels were calculated by the equation [37]:

$$L_p = 10\log\left(E_f/0.07\ p_h^2\right) - 3, \qquad (10)$$

where $p_h = 20$ μPa. These pressure levels were further reduced to equivalent loudness levels in dB for a frequency of 3150 Hz using equal loudness curves, according to which the highest hearing sensitivity falls in the interval from 1 to 5 kHz [36–38]. From the equivalent loudness levels in decibels, the loudness in sones was calculated and the maximum loudness among all one-third octave bands was found. Next, the algorithm calculates the resulting integral loudness parameter in sones, simulating the masking features of human hearing: the maximum loudness over all one-third octave bands is taken into account with a weight equal of 1; the summed loudness over all the remaining bands, with a weight that depends on the maximum loudness; and in the case of sonic boom, ~0.2. At the final step, the resulting loudness in sones is converted to decibels. The PL calculation algorithm was tested by comparing the results for a waveform digitized from a printed figure from [38]. The comparison showed that the results differ by less than 0.2 dB.

For the initial N-wave waveforms used in this work, the PL values were: 76.8 dB for $p_0 = 10$ Pa, 89.5 dB for $p_0 = 20$ Pa, and 101 dB for $p_0 = 40$ Pa. Clearly, with doubling of the N-wave amplitude, the subjective loudness does not increase by 6 dB, as it would in the case of a sinusoidal signal, but approximately twice as much, by 12.6 dB between cases with $p_0 = 10$ Pa and $p_0 = 20$ Pa, and by 11.5 dB between cases with $p_0 = 20$ Pa and $p_0 = 40$ Pa. The 12 dB difference is explained by the fourfold increase in the average steepness of the shock front for doubling p_0 [47].

The maximum steepness of the waveform was calculated using the algorithm described in [30]. In this algorithm, the time derivative of the waveform is calculated first. Next, the maximum of the derivative is searched over the entire waveform, which, as a rule, corresponds to the strongest and steepest shock front in the waveform. Then, to the left and to the right of the maximum of the derivative are points lying at a level of 0.3679 from the maximum. The points are used to calculate the time interval, which is taken as the rise time of the shock front, as well as the drop in pressure at the front. The steepness of the shock front is determined as the ratio of the drop in pressure across the front to the rise time of the front.

Note that the PL considered in the study was introduced to mainly assess the influence of the high-frequency components of the sonic boom wave spectrum responsible for the perceived loudness level. It was demonstrated that this metric is preferable for analysis of sonic boom waves when a person is outdoors [34, 35]. The design of new generation of supersonic aircraft is aimed at reducing the characteristic PL levels by generating a modified sonic boom wave (low boom) with larger shock front rise time and, accordingly, a lower energy component in the high-frequency region. At the same time, the need to introduce additional metrics is also discussed in order to assess the perception of the low-frequency components of the modified sonic boom by a person both out- and indoors, including rumbling and vibrations from objects and structural elements [35, 39].

2.6. Statistical Data Analysis

At each step of the algorithm along the z axis, all the acoustic field parameters of interest were calculated over the entire width of the computational domain along the transverse axis x, except for buffer zones near its edges: positive peak pressure (amplitude) p_{max}, steepness of the shock front s_{max}, and PL. All parameters were normalized to the values obtained for the same initial data when calculating the propagation of an N-wave in a homogeneous medium: p_{ref}, s_{ref}, and PL_{ref}, respectively. The obtained distributions of the normalized parameters along the x axis were used to calculate the mean value, standard deviation, and histograms of probability distribution functions. The histograms were used to find the values of the cumulative probability of the parameter exceeding a given threshold.

In total, for each numerical experiment with a given amplitude of the initial N-wave waveform, two independent random realizations of turbulence were used, with a width of 11800 m each. This realization size corresponds to a transverse length of the compu-

tational domain of 12800 m minus 1000 m of buffer zones, 500 m on each side. Statistical data from each realization from a set of two realizations were combined.

3. RESULTS AND DISCUSSION

3.1. Spatial Distributions of N-wave Parameters

Figure 2 shows examples of the spatial distributions of the wind speed modulus, amplitude, steepness of the shock front, and PL in a domain of 2 × 2 km. The wind speed is normalized to the sound speed (Fig. 2a); the amplitude (Fig. 2b), steepness of the shock front (Fig. 2c) and PL (Fig. 2d) are normalized to the corresponding values obtained during *N*-wave propagation in a homogeneous medium (p_{ref}, s_{ref} and PL_{ref}). All distributions of the acoustic field parameters are generally similar to each other: they show the formation of random caustics of various intensities and at different distances deep in the turbulent layer. In the caustics, as a rule, increased amplitude, steepness, and PL values are observed. In regions between the caustics, there are defocusing regions, where these parameters are reduced with respect to the nominal values. However, the distributions differ in detail. For example, on the distributions of the steepness of the shock front and PL, the focal maxima are found more frequently along the transverse coordinate than on the distributions of amplitude. It is also seen that the characteristic focusing gain for the amplitude in the caustics is 2–3, and for the steepness of the shock front, 3–4. The spread in PL from −14 to +10 dB corresponds to the data obtained in field experiments [17]. Exact quantitative relationships can be derived from statistical analysis of the data presented in the next two sections.

Figure 3 shows examples of typical sonic boom waveforms normalized to pressure p_0 after propagation through a turbulent layer of 2 km thickness for different initial *N*-wave amplitudes: the solid black curve corresponds to p_0 = 10 Pa; the blue dashed curve, to p_0 = 20 Pa; and the red dash–dot curve, to p_0 = 40 Pa. The same color scheme will be used below for results obtained for different *N*-wave amplitudes. On the waveforms, it is often possible to detect small pressure peaks immediately behind the shock front (Fig. 3a); in the defocusing regions, the waveform is smoothed and has a reduced amplitude (Fig. 3b); in the vicinity of caustics, the waveform has an increased amplitude (Fig. 3c), and the waveform contains two or more steps, which is explained by the folding effect of the wave front in the caustics [15]. The normalized waveforms obtained for different initial amplitudes differ mainly in the steepness of the shock fronts. The low-frequency part of the waveforms is nearly the same.

3.2. Mean Value and Standard Deviation of N-wave Parameters

Figure 4 shows mean values and standard deviations of the *N*-wave parameters as functions of the propagation distance z for the normalized values of the amplitude (Fig. 4a), steepness of the shock front (Fig. 4b), and PL (Fig. 4c). The mean values are shown by thin curves; standard deviations, by thick curves. Different curve colors and shading correspond to different initial *N*-wave amplitudes: black solid curve, p_0 = 10 Pa; blue dashed curve, p_0 = 20 Pa; red dash-dot curve, p_0 = 40 Pa.

The mean value of amplitude compared to the nominal level increases with increasing z. This is due to the formation of peaks in the waveforms in caustics with different focusing gains (Figs. 3a, 3c). The degree of increase of the mean amplitude compared to the nominal level increases with initial amplitude and for z = 2 km is 1.15; for p_0 = 10 Pa, 1.26; for p_0 = 20 Pa; and for p_0 = 40 Pa, 1.37. This is because the rise time of the shock front decreases and its steepness increases with increasing p_0, which leads to more efficient focusing in caustics.

The standard deviation of the wave amplitude increases with the distance z as new caustics form with focusing by randomly scattered "lenses" of different scales and strengths. At a certain distance corresponding to focusing from the largest-scale inhomogeneities (in this case, 1.5 km), the standard deviation reaches a maximum, the value of which also depends on the amplitude and steepness of the shock front of the initial *N*-wave. The higher the focusing efficiency in caustics, the higher fluctuations of the amplitude and, accordingly, the standard deviation, the maximum of which is 0.29 for p_0 = 10 Pa, 0.36 for p_0 = 20 Pa, and 0.48 for p_0 = 40 Pa.

A similar behavior of the mean value and standard deviation of the amplitude depending on the propagation distance was found earlier in laboratory experiments on shock wave propagation from a spark source through a thermal or kinematic turbulence layer [19, 20] and in simulations of these experiments with the nonlinear parabolic equation used in this study [28, 30]. The differences between the laboratory and real scale data are mostly quantitative. For example, in laboratory experiments and corresponding calculations, the mean value of the amplitude never exceeded the nominal level. This is because the characteristic frequencies of the shock wave from the spark source are three to four orders of magnitude higher than those of a sonic boom wave. At such high frequencies, thermoviscous absorption becomes the dominant absorption mechanism, in contrast to the relaxation mechanism, which governs the structure of the shock front in real scale conditions. In that case, the shock front from the spark source at the inhomogeneity scales used (10–20 cm)

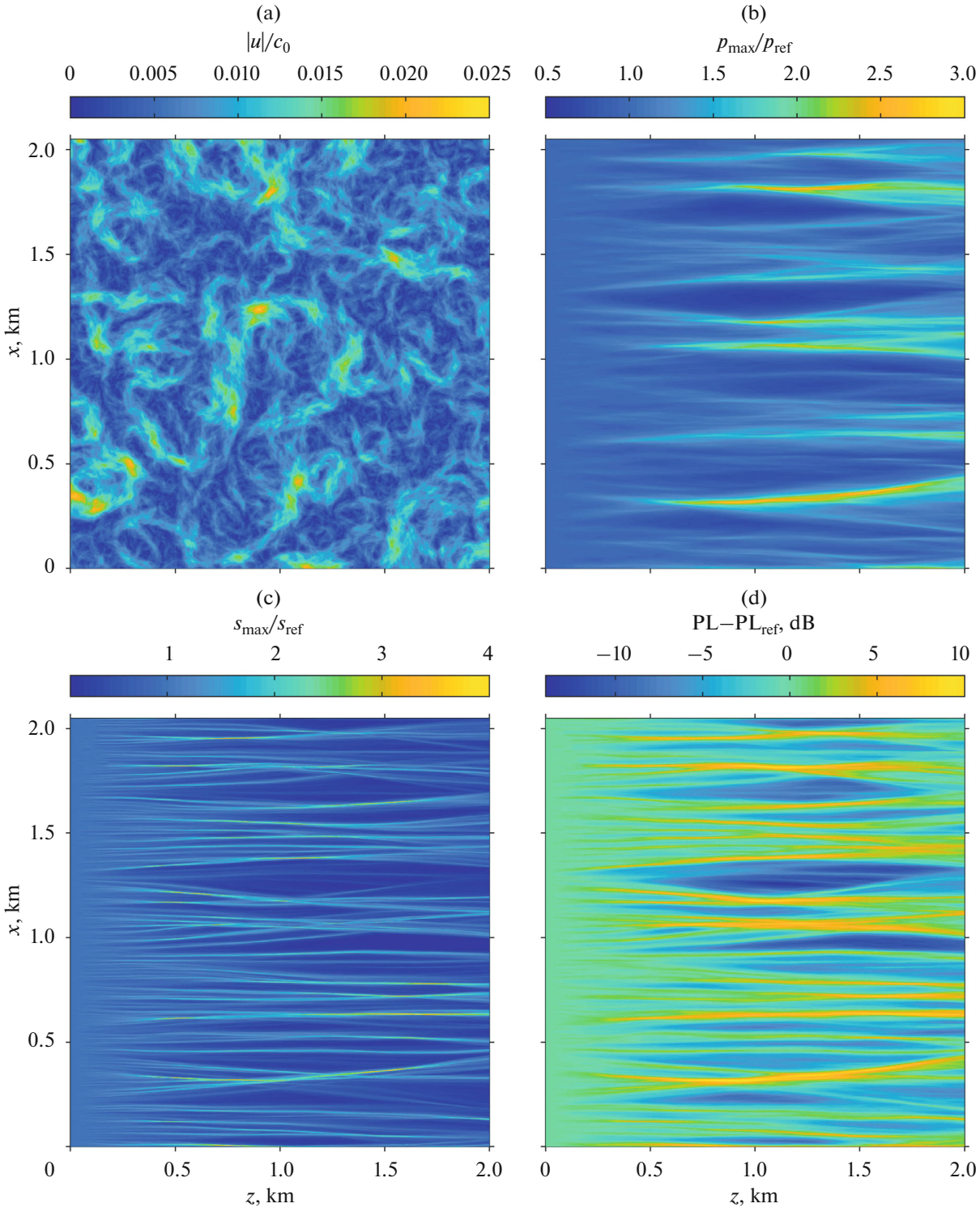

Fig. 2. Spatial distributions of (a) wind speed modulus normalized to the sound speed, (b) shock wave amplitude, (c) steepness of the shock front, and (d) PL, normalized to the corresponding values obtained during propagation of the plane wave in homogeneous medium. Distributions correspond to the case of N-wave with initial amplitude $p_0 = 20$ Pa.

becomes quite large (1 μs or higher), which reduces the focusing efficiency in caustics.

The mean value of the steepness of the shock front decreases compared to the nominal level with increasing distance traveled by the wave (Fig. 4b). This process occurs the faster, the larger the amplitude of the initial wave and is explained by the fact that the steeper front is more easily blurred with multiple scattering by

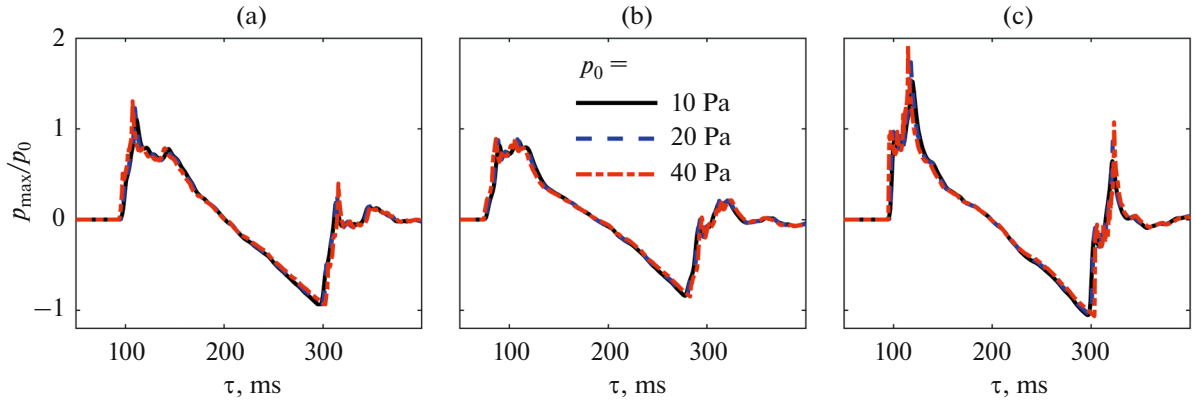

Fig. 3. Examples of sonic boom waveforms after propagation through a turbulent layer of 2 km thickness for different initial N-wave amplitudes: solid black curve, $p_0 = 10$ Pa; blue dashed curve, $p_0 = 20$ Pa; red dash-dotted curve, $p_0 = 40$ Pa. N-wave waveforms: (a) with a peak near the shock front, (b) in defocusing region, (c) with a large amplitude near caustics.

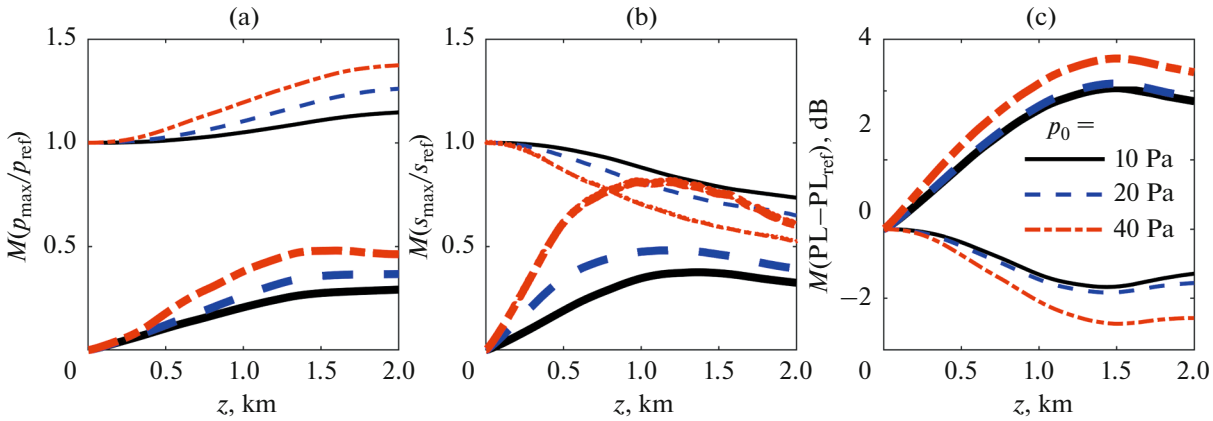

Fig. 4. Mean values (thin curves) and standard deviations (bold curves) for (a) normalized amplitude, (b) steepness of the shock front, and (c) PL as functions of distance z traveled for different initial N-wave amplitudes: solid black curve, $p_0 = 10$ Pa; blue dashed curve, $p_0 = 20$ Pa; red dash-dotted curve, $p_0 = 40$ Pa.

random medium and small-scale inhomogeneities. In simulating laboratory experiments, the dependence of the average steepness on the initial wave amplitude was the inverse [30], which most likely follows from the fact that the effects of nonlinear steepening of the waveform under such conditions played a greater role than in the case of a sonic boom wave. The standard deviation of steepness of the shock front increases and reaches a peak similarly to the standard deviation of amplitude. However, this occurs somewhat closer to the beginning of the layer (at $z = 0.9$–1.2 km) compared to the position of the maxima of the standard deviation of the amplitude. In that case, the achieved maxima of the standard deviation of the steepness of the shock front are 0.38 for $p_0 = 10$ Pa, 0.48 for $p_0 = 20$ Pa, and 0.81 for $p_0 = 40$ Pa. These values are 25–30% ($p_0 = 10$ Pa and $p_0 = 20$ Pa) and 80% ($p_0 = 40$ Pa) greater than the corresponding standard deviations of the amplitude, which means that the steepness of the shock front fluctuates more strongly than the amplitude, and the magnitude of fluctuations increases with increasing amplitude and steepness of the shock front of the initial N-wave. This qualitative conclusion coincides with that for the curves of the standard deviation of the steepness of the shock front in laboratory-scale turbulence [30].

The mean value of PL decreases on the whole with increasing distance traveled by the wave, and only closer to $z = 2$ km there is a tendency toward a slight increase. The maximum drop in mean loudness for the cases $p_0 = 10$ Pa and $p_0 = 20$ Pa hardly depends at all on the amplitude of the initial N-wave: -1.8 dB. For the case $p_0 = 40$ Pa, the drop in mean loudness is greater: -2.7 dB. The standard deviation of PL increases, reaching a maximum at approximately the same distances where the maximum standard deviation of the amplitude is observed ($z = 1.5$ km). The maximum of the standard deviation of PL reaches

4.2 dB and is virtually independent of the amplitude of the initial N-wave for the cases $p_0 = 10$ Pa and $p_0 = 20$ Pa. For $p_0 = 40$ Pa, the maximum standard deviation is greater: 5.0 dB. This will be explained following the discussion of cumulative probabilities in the next section.

3.3. Cumulative Probabilities of the N-wave Parameters

The mean value and standard deviation provide only generalized information about a random variable if the latter is not Gaussian. As shown earlier in experimental and theoretical studies, the amplitude distribution has "tails" in the direction of large values from the mean value, as indicated by the positive value of the asymmetry coefficient [28]. The amplitude distribution can be approximated by a generalized Γ-distribution [19]. The distribution of the steepness of the shock front is also non-Gaussian. According to the calculations in this work, in the region where caustics are formed ($z > 1$ km), the asymmetry and kurtosis coefficients of distribution of steepness of the shock front are greater than 1 for all three cases. Only the PL distribution is closest to Gaussian: the asymmetry and kurtosis coefficients change sign as the wave propagates, but do not exceed 0.5 and 0.8 in absolute value, respectively.

From the aspect of the procedures for certifying supersonic aircraft in terms of noise level, it is very important to assess the probability of the nominal level being exceeded by a given threshold value. Based on the data on the characteristic focusing gain values of various parameters of the wave field in caustics (Fig. 2), it makes sense to choose excess thresholds for the normalized amplitude and steepness of the shock front of 2, and for the PL metric, as corresponding to a twofold increase in amplitude of +6 dB.

Figure 5 shows the cumulative probabilities of exceeding the specified thresholds for the normalized values of the amplitude (Fig. 5a), the steepness of the shock front (Fig. 5b) and PL (Fig. 5c) as functions of the propagation distance z for different initial N-wave amplitudes. Up to certain distances z, different for different parameters and p_0 values, the probabilities are zero until caustics with a sufficient focusing gain are formed. Then, the probabilities begin to increase, and at some distance, the maximum is reached. For the amplitude, this is from 1.5 to 2 km; for the steepness of the front, 0.8–1.1 km; for PL, 1.2–1.4 km, which actually corresponds to the distances at which the maxima of the standard deviation of each of the considered quantities are formed (Fig. 4). It can be emphasized that the maxima of the probability of the amplitude and steepness strongly depend on the amplitude of the initial N-wave waveform. For $p_0 = 10$ Pa, less than 0.9% of the waveforms have an amplitude that is twice the nominal level. With twofold increase of the initial amplitude $p_0 = 20$ Pa, the number of such waveforms can be up to 4.3%, and with a fourfold greater amplitude $p_0 = 40$ Pa, up to 10.6%. For the steepness of the shock front, the corresponding maximum probabilities in order of increasing N-wave amplitude are 1.0, 2.6, and 6.3%. This behavior of the cumulative probabilities of observing high values for the amplitude and steepness of the shock front is explained by an increase in the focusing efficiency in random caustics due to the steepness of the shock front of the initial wave that passed through a focusing inhomogeneity. Nonlinear effects support the structure of the shock front, preventing it from significant blurring due to multiple instances of scattering by inhomogeneities of various scales and strengths [14, 48]. In that case, with increasing amplitude in caustics, the role of nonlinear effects increases.

In contrast to the cumulative probabilities of amplitude and steepness of the shock front, the variability of the cumulative probability curve of PL is nearly independent of the initial N-wave amplitude for cases with $p_0 = 10$ Pa and $p_0 = 20$ Pa. The maximum probability does not exceed 3%, which actually means that only every 30th waveform is 6 dB louder than the nominal one. After passing a distance at which the strongest caustics are formed (here it is about 1.5 km), at $z = 2$ km, the probability drops to 1.4%. The maximum probability of obtaining a sonic boom wave with a loudness of 10 dB greater than the nominal one is less than 0.1% and in practice can be considered zero. For $p_0 = 40$ Pa, the maximum probability becomes greater: 4.4%. For $z = 2$ km, the probability drops to 2.3%. The maximum probability of obtaining a sonic boom wave with a loudness of 10 dB greater than the nominal one in this case is less than 0.4%, which can also be considered insignificant.

The weak sensitivity of the cumulative probability of the normalized PL to the initial N-wave amplitude for $p_0 = 10$ Pa and $p_0 = 20$ Pa, and, accordingly, to an increased steepness of the waveform in caustics (Fig. 5b), is explained by the features of the change in the N-wave spectrum with an increase in its amplitude, as well as by the method for taking into account the loudness inherent in the PL calculation algorithm. Figure 6 shows the influence of the wave amplitude. The gray curves show the sound pressure levels in the one-third octave bands, calculated by formula (10) for the initial N-wave waveforms (thick gray curves). It can be seen that whereas at low frequencies the sound pressure level increases by 6 dB when the amplitude is doubled, starting from frequencies above several hundred hertz, a significantly greater rise in the pressure level is observed (see the difference between the gray curves). This effect is due to the decrease in the rise time of the shock front and an increase in its steepness, which increases in proportion to the wave amplitude squared. The colored curves show the average sound pressure levels for waves distorted in a turbulent layer at a distance $z = 1.5$ km, which corresponds to the

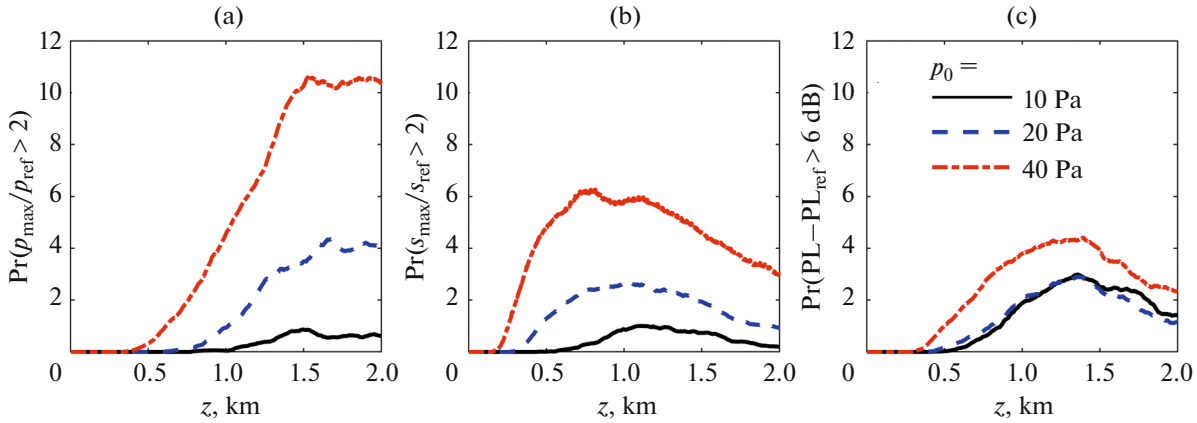

Fig. 5. Cumulative probabilities of exceeding a given threshold for (a) normalized amplitude, (b) steepness of the shock front, and (c) PL as functions of distance z traveled for different initial N-wave amplitudes: solid black curve, $p_0 = 10$ Pa; blue dashed curve, $p_0 = 20$ Pa; red dash-dotted curve, $p_0 = 40$ Pa. For amplitude and steepness of the shock front, threshold is set to 2; for PL, 6 dB.

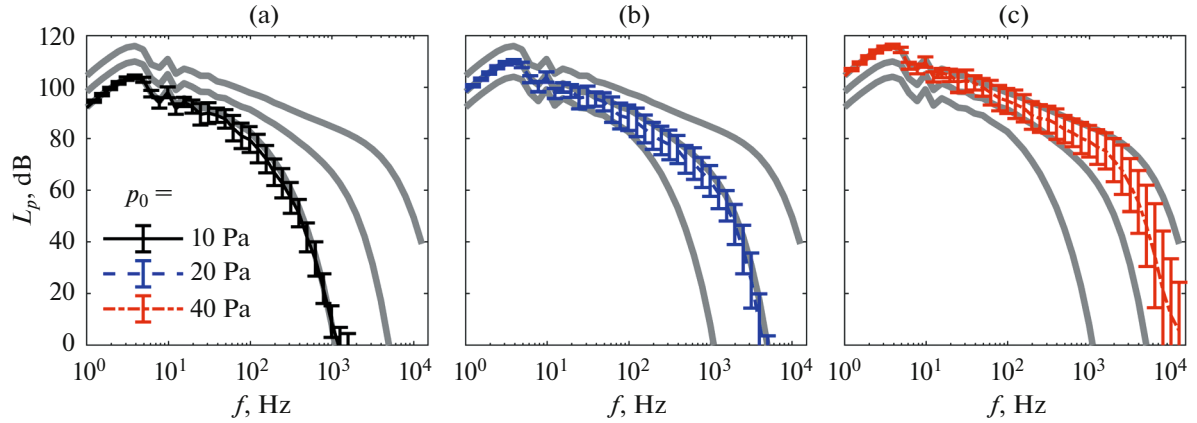

Fig. 6. One-third octave bands sound pressure level curves in dB, calculated for initial N-wave waveforms with amplitudes of 10, 20, and 40 Pa (bold gray curves) and average values for waves distorted in turbulent layer at distance $z = 1.5$ km, which corresponds to the maximum PL fluctuations. Vertical intervals denote standard deviation of sound pressure level. Solid black curve corresponds to (a) $p_0 = 10$ Pa; blue dashed curve (b), $p_0 = 20$ Pa; red dash-dotted curve (c), $p_0 = 40$ Pa.

maximum PL fluctuations; the vertical intervals show the standard deviation of the sound pressure level. Clearly, in the low-frequency region (up to 10 Hz), turbulence-related spectral fluctuations are insignificant. At higher frequencies (from 10 Hz and above), appreciable fluctuations occur.

Then, based on the sound pressure levels in one-third octave bands, the PL algorithm calculates the subjective loudness levels, measured in sones, the plots of which corresponding to the spectra in Fig. 6 for the initial waveforms and for the waveforms in a turbulent layer at a distance of 1.5 km are shown in Fig. 7. Since calculation of the subjective loudness takes into account an increase in hearing sensitivity with increasing frequency, despite the general drop in the sound pressure level starting at 5 Hz (Fig. 6), there is a clear maximum on the loudness graphs. For waves with initial amplitudes of 10 and 20 Pa, the loudness maximum is near frequency 100 Hz, i.e., lower than the characteristic frequencies of shock fronts. This is also illustrated in Fig. 7b by the green dashed curve, representing the loudness curve for the initial N-wave waveform for $p_0 = 10$ Pa, but with double the amplitude. The steepness of the shock front of such a wave is two times less than the steepness of the shock front of the initial wave with an amplitude of 20 Pa and with a physically substantiated shock front structure. It can be seen that the maximum in the loudness spectrum shifts slightly, from 80 Hz for $p_0 = 10$ Pa to 124 Hz for $p_0 = 20$ Pa, and the increase in loudness due to the increased steepness of the shock front occurs at higher frequencies. The maximal loudness fluctuations center around the maximum of the average loudness curve over one-third octave bands. Therefore, when calcu-

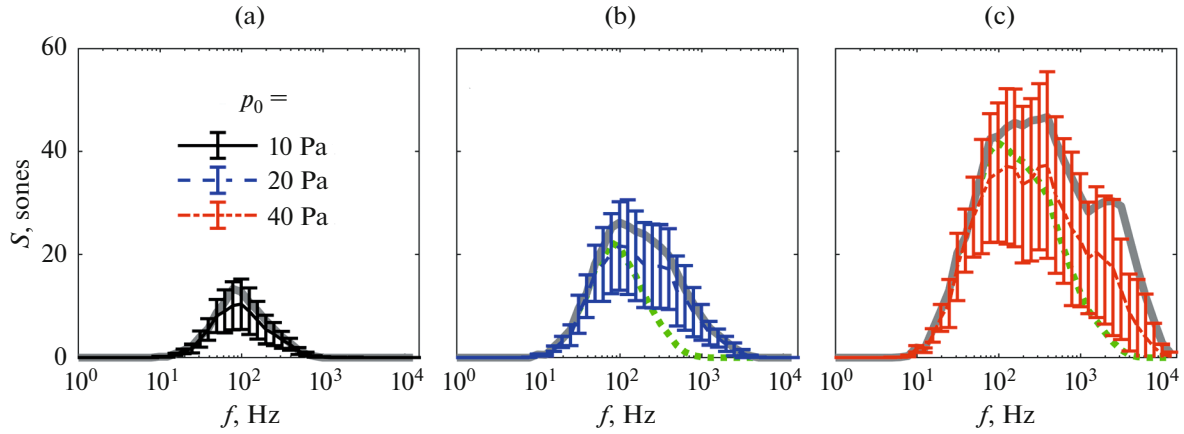

Fig. 7. Curves of subjective loudness level, measured in sones, in one-third octave bands, calculated for initial N-wave waveforms with amplitudes of 10, 20, and 40 Pa (thick gray curves) and average values for waves distorted in turbulent layer at distance z = 1.5 km, which corresponds to maximum PL fluctuations. Vertical intervals show standard deviation of loudness level. Solid black curve (a), p_0 = 10 Pa; blue dashed curve (b), p_0 = 20 Pa, red dash-dotted curve (c), p_0 = 40 Pa. Green dashed line (b) shows loudness levels in one-third octave bands, calculated for initial N-wave waveform for p_0 = 10 Pa with doubled amplitude without change in structure of shock front; green dash-dotted line in (c) is same, but for case of p_0 = 20 Pa.

lating PL, a loudness of ~100 Hz will make a decisive contribution. And since these frequencies do not correspond to the characteristic shock front frequencies, fluctuations around the mean value will behave similarly, regardless of the shock front parameters.

For an initial wave amplitude of 40 Pa, the maximum of the spectral loudness curve shifts to higher frequencies, about 400 Hz, compared to the initial amplitudes of 10 and 20 Pa. From the loudness curve for the N-wave obtained for the initial one from the waveform with p_0 = 20 Pa by simply doubling the amplitude (Fig. 7c, dashed green curve), it can be seen that an increase in loudness in one-third octave bands due to the steepness of the front occurs at frequencies from hundreds of hertz to 10 kHz. As a result of the shift in the maximum of the spectral loudness curve to the higher-frequency region, where effects related to fluctuations in the steepness of the shock front and the corresponding high-frequency spectral components are more substantial, nonlinear effects have a stronger effect on the PL statistics. This process is reflected in the curves of the mean, standard deviation (Fig. 4c), and cumulative probability (Fig. 5c).

4. CONCLUSIONS

In this paper, propagation of a sonic boom with a classical N-wave waveform through atmospheric turbulent layer was analyzed using numerical modeling methods. The effect of the initial wave amplitude in the range of 10–40 Pa on the statistics of the acoustic field parameters was evaluated. Peak positive pressure (amplitude), steepness of the shock front, and loudness metric PL were considered as sonic boom parameters and cumulative probabilities of their twofold excess were calculated with respect to the nominal level. It was shown that an increase in the initial N-wave amplitude leads to a significant increase in the probability of positive outliers for the amplitude and steepness of the shock front. These effects are related to increased efficiency of the shock front focusing in random caustics with an increased role of nonlinear effects. In this case, the probability of positive outliers for PL hardly changes for initial wave pressures of 10 and 20 Pa (3%) and increases with increasing amplitude to 40 Pa (4%). This PL behavior is explained by the shift in the spectral loudness curve, starting from a certain level of steepness of the shock front, to the high frequencies of increased human hearing, and the emphasis on the weight of these frequencies when constructing the metric. Thus, reducing the amplitude of a sonic boom not only reduces the nominal subjective noise level, but also reduces the likelihood of observing its positive outliers. The results demonstrate the importance of developing the concept of supersonic aircraft with low-noise sonic boom waveforms with a smaller steepness of the front and lower level of high-frequency spectral components.

FUNDING

The study was supported by a grant from the Russian Science Foundation (no. 18-7200196). Ph. Blanc-Benon was supported by the LABEX CeLyA (ANR-10-LABX-0060/ANR-16-IDEX-0005).

ACKNOWLEDGMENTS

The authors are grateful to L.R. Gavrilov for helpful discussions and comments.

REFERENCES

1. D. Maglieri, P. Bobbitt, K. Plotkin, K. Shepherd, P. Coen, and D. Richwine, NASA Technical Report (NASA, 2014), No. NASA/SP-2014-622, L-20381, NF1676L-18333, p. 521.
2. S. L. Chernyshev, *Sonic Boom* (Nauka, Moscow, 2011) [in Russian].
3. V. A. Krasil'nikov, Acoust. Phys. **44** (4), 481 (1998).
4. J. A. Page and A. Loubeau, CEAS Aeronaut. J. **10**, 335 (2019).
5. L. R. Benson, *Quieting the Boom: The Shaped Sonic Boom Demonstrator and the Quest for Quiet Supersonic Flight* (NASA, 2019), p. 388.
6. T. Feder, Phys. Today **60** (4), 24 (2007).
7. R. Cowart and T. Grindle, in *Proc. 46th AIAA Aerospace Sciences Meeting and Exhibition* (Reno, NV, Jan. 7–10, 2008), No. AIAA 2008–123.
8. V. I. Biryuk, M. R. Ibragimov, V. V. Kovalenko, A. P. Novikov, V. N. Titov, T. Yu. Chaika, Yu. N. Chernavskikh, and V. G. Yudin, Uch. Zap. TsAGI **41** (5), 13 (2010).
9. V. V. Kovalenko and S. L. Chernyshev, Uch. Zap. TsAGI **37** (3), 53 (2006).
10. S. L. Chernyshev, A. P. Kiselev, and P. P. Vorotnikov, in *Proc. 46th AIAA Aerospace Sciences Meeting and Exhibition* (Reno, NV, Jan. 7–10, 2008), No. AIAA 2008–58, p. 18.
11. F. Alauzet and A. Loseille, J. Comput. Phys. **229**, 561 (2010).
12. V. E. Ostashev and D. K. Wilson, *Acoustics in Moving Inhomogeneous Media*, 2nd ed. (CRC Press Taylor & Francis Group, 2016), p. 521.
13. R. A. Lee and J. M. Downing, J. Acoust. Soc. Am. **99** (2), 768 (1996).
14. A. Pierce and D. Maglieri, J. Acoust. Soc. Am. **51**, 702 (1972).
15. A. A. Piacsek, J. Acoust. Soc. Am. **111** (1(2)), 520 (2002).
16. D. J. Maglieri, J. Acoust. Soc. Am. **39**, 36 (1966).
17. K. R. Elmer and M. C. Joshi, NASA Contractor Report (1994), Vol. 1, No. 191483.
18. B. Lipkens and D. Blackstock, J. Acoust. Soc. Am. **103** (1), 148 (1998).
19. M. Averiyanov, S. Ollivier, V. A. Khokhlova, and Ph. Blanc-Benon, J. Acoust. Soc. Am. **130** (6), 3595 (2011).
20. E. Salze, P. V. Yuldashev, S. Ollivier, V. A. Khokhlova, and Ph. Blanc-Benon, J. Acoust. Soc. Am. **136** (2), 556 (2014).
21. V. W. Sparrow and A. D. Pierce, in *High-Speed Research: Sonic Boom,* (1992), Vol. 1, NASA Conference Publication 3172, p. 49.
22. Yu. A. Zavershnev, A. V. Rodnov, and S. L. Chernyshev, Tr. Tsentr. Aerogidrodin. Inst. im. Professora N. E. Zhukovskogo, No. **2670**, 91 (2005).
23. S. L. Chernyshev, Uch. Zap. TsAGI, **27** (3), 10 (2006).
24. V. A. Gusev and O. V. Rudenko, Acoust. Phys. **52** (1), 24 (2006).
25. A. N. Dubrovskii, O. V. Rudenko, and V. A. Khokhlova, Acoust. Phys. **42** (5), 550 (1996).
26. M. V. Aver'yanov, V. A. Khokhlova, O. A. Sapozhnikov, Ph. Blanc-Benon, and R. Cleveland, Acoust. Phys. **52** (6), 623 (2006).
27. Ph. Blanc-Benon, B. Lipkens, L. Dallois, M. F. Hamilton, and D. T. Blackstock, J. Acoust. Soc. Am. **111** (1), Pt. **2**, 487 (2002).
28. M. V. Averiyanov, Ph. Blanc-Benon, R. Cleveland, and V. A. Khokhlova, J. Acoust. Soc. Am. **129** (4), 1760 (2011).
29. T. A. Stout and V. W. Sparrow, J. Acoust. Soc. Am. **144** (2), EL229 (2018).
30. P. V. Yuldashev, S. Ollivier, M. M. Karzova, V. A. Khokhlova, and Ph. Blanc-Benon, J. Acoust. Soc. Am. **142** (6), 3402 (2017).
31. D. Luquet, R. Marchiano, and F. Coulouvrat, J. Comput. Phys. **379**, 237 (2019).
32. L.-J. Gallin, M. Renier, E. Gaudard, T. Farges, R. Marchiano, and F. Coulouvrat, J. Acoust. Soc. Am. **135** (5), 2559 (2014).
33. I. G. Bashkirov, S. L. Chernyshev, V. S. Gorbovskoy, A. V. Kazhan, V. G. Kazhan, and V. V. Kovalenko, in *Proc. 9th EASN Int. Conf. on "Innovation in Aviation & Space"* (Athens, 2019), Vol. 304, p. 02003.
34. J. Leatherwood, B. Sullivan, K. Shepherd, D. McCurdy, and S. Brown, J. Acoust. Soc. Am. **111** (1(2)), 586 (2002).
35. A. Loubeau, Y. Naka, B. G. Cook, V. W. Sparrow, and J. M. Morgenstern, AIP Conf. Proc., No. 1685, 090015-1 (2015).
36. S. S. Stevens, J. Acoust. Soc. Am. **51**, 575 (1972).
37. G. Jackson and H. Leventhall, Appl. Acoust. **64**, 23 (1973).
38. C. R. Bolander, D. F. Hunsaker, H. Shen, and F. L. Carpenter, in *Proc. AIAA SciTech Forum* (San Diego, Jan. 7–11, 2019), p. 1.
39. W. J. Doebler and V. W. Sparrow, J. Acoust. Soc. Am. **141** (6), 592 (2017).
40. A. D. Pierce, *Acoustics: An Introduction to Its Physical Principles and Applications* (Springer, 2019), p. 768.
41. G. Comte-Bellot and C. Bailly, *Turbulence* (CNRS, Paris, 2003), p. 360.
42. F. Coulouvrat, in *Proc. 15th AIAA/CEAS Aeroacoustics Conf. (30th AIAA Aeroacoustics Conf.)* (Miami, May 11–13, 2009), No. AIAA. 2009–3384.
43. A. L. Polyakova, S. I. Soluyan, and R. V. Khokhlov, Akust. Zh. **8** (1), 107 (1962).
44. H. E. Bass, R. Raspet, J. P. Chambers, and M. Kelly, J. Acoust. Soc. Am. **111** (1(2)), 481 (2002).
45. P. V. Yuldashev, S. Ollivier, M. V. Averiyanov, O. A. Sapozhnikov, V. A. Khokhlova, and Ph. Blanc-Benon, J. Acoust. Soc. Am. **128** (6), 3321 (2010).
46. R. J. Zemp, J. Tavakkoli, and R. S. Cobbold, J. Acoust. Soc. Am. **113** (1), 139 (2003).
47. K. P. Shepherd and B. M. Sullivan, NASA Technical Paper (1991), No. 3134, p. 1.
48. P. V. Yuldashev, M. M. Karzova, S. Ollivier, V. A. Khokhlova, and Ph. Blanc-Benon, in *Proc. 25th AIAA/CEAS Aeroacoustics Conf.* (Delft, May 20–23, 2019), No. AIAA 2019–2563.